Inorganic Chemistry

ARTICLE

pubs.acs.org/IC

Synthesis of Uniform and Dispersive Calcium Carbonate Nanoparticles in a Protein Cage through Control of Electrostatic Potential

Hiroko Fukano,[†] Takuya Takahashi,[‡] Mamoru Aizawa,[§] and Hideyuki Yoshimura*[,†]

[†]Department of Physics and [§]Department of Applied Chemistry, Meiji University, 1-1-1 Higashi-mita, Tama-ku, Kawasaki, Kanagawa 214-8571, Japan

[‡]Department of Bioscience and BioInformatics, Graduate School of Science and Engineering College of Life Sciences, Ritsumeikan University, 1-1-1 Noji-higashi, Kusatsu, Shiga 525-8577, Japan

ABSTRACT: We have synthesized calcium carbonate nanoparticles (Ca-NPs) in the cavity of a cage-shaped protein, apoferritin, by regulating the electrostatic potential of the molecule. The electrostatic potential in the cavity was controlled by pH changes resulting from changes in the dissolved carbon dioxide (CO_2) concentration in the reaction solution. Recombinant L-apoferritin was mixed with a suspension of calcium carbonate ($CaCO_3$), and the mixture was pressurized with gaseous CO_2 at 2 MPa. The pH of the solution decreased from 9.3 to 4.4; the $CaCO_3$ dissolved during pressurization, and then precipitated after the pressure was reduced to ambient. After repeating the pressurization/depressurization process three times, about 70% of the apoferritin molecules were found to contain nanoparticles with an average diameter of 5.8 ± 1.2 nm in their cavity. Energy-dispersive X-ray spectroscopy and electron diffraction analysis showed that the nanoparticles were calcite, one of the most stable crystal forms of $CaCO_3$. Electrostatic potential calculations revealed a transition in the potential in the apoferritin cavity, from negative to positive, below pH 4.4. The electrostatic potential change because of the change in pH was crucial for ion accumulation. Since the Ca-NPs synthesized by this method were coated with a protein shell, the particles were stably dispersed in solution and did not form aggregates. These Ca-NPs may be useful for medical applications such as synthetic bone scaffolds.

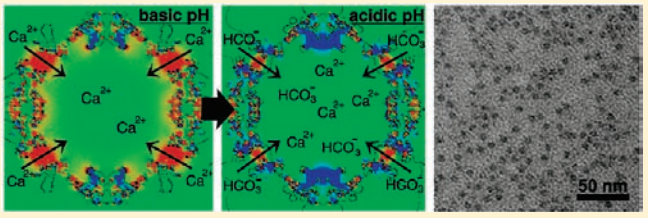

INTRODUCTION

Naturally formed biomaterials such as bones, teeth, and shells have regular hierarchical structure. Because of their unique structures, their mechanical strength and functional properties are often superior to artificial materials. This has attracted great interest in developing mineralized biologically inspired materials.[1] Because proteins play an important role in biomineralization, synthesis methods using proteins as templates are an interesting strategy for the fabrication of high performance materials.[2,3] Here, we report a new fabrication method for calcium carbonate nanoparticles (Ca-NPs) using the protein apoferritin as a template.

Apoferritin, an iron storage protein found in many biological species, mineralizes several metal ions in vitro.[4] It is a hollow, spherical protein composed of 24 subunits, with outer and inner diameters of 13 and 7.4 nm, respectively. The apoferritin cavity can deposit up to 4500 iron atoms as a ferrihydrite.[5] Apoferritin is composed of two types of subunits, a light-chain subunit (L-subunit) and a heavy-chain subunit (H-subunit). The sequence identity between the L-subunit and H-subunit in human apoferritin is 53%, and their three-dimensional structures are very similar. In this study, we used native horse spleen apoferritin (HSAF), recombinant horse L-apoferritin (apofer-0), and a mutant of recombinant horse L-apoferritin (apofer-8). HSAF is composed of about 85% L-subunits and 15% H-subunits.[5] Apofer-0 is a recombinant protein cloned from cDNA of the L-subunit of horse liver apoferritin, and thus is composed only of the L-subunit. Apofer-8 is a mutant of apofer-0 and is used as a model of the HSAF L-subunit. Because of post-translational modification, the L-subunit of HSAF lacks the eight amino acid residues at the N-terminus of apofer-0.[6] The apoferritin molecule has *F*432 symmetry, and eight hydrophilic channels along the 3-fold symmetry axes (3-fold channels) connect the apoferritin cavity to the outer bulk solution.[7] These channels are believed to allow the passage of metal ions in and out of the cavity. Six hydrophobic channels along the 4-fold symmetry axes (4-fold channels) may act as outlets for protons during oxidation.[8] Eight amino acid residues at the N-terminus of apofer-0 bridge two neighboring subunits and stabilize the apoferritin molecule.[9] Because of the deletion of this fragment in apofer-0, the ion channels formed by the intersubunit openings would fluctuate more in apofer-8 than apofer-0. Therefore, apofer-8 shows more efficient nanoparticle formation than apofer-0. Most metal mineralization studies have been performed using apofer-8 or HSAF.[10,11]

Many transition metals have been mineralized in oxidized or hydrated forms in the apoferritin cavity, but there have been few reports of alkaline earth metal mineralizations. Recently, Li

Received: January 19, 2011
Published: June 15, 2011

ACS Publications © 2011 American Chemical Society

et al.[12] reported alkaline earth metal carbonate mineralization using HSAF with the help of an anionic polymer [poly(methacrylic acid)], but we could not reproduce their results, perhaps because the free calcium ion concentration must be precisely controlled. We therefore tried to establish another strategy for calcium mineralization by controlling the CO_2 concentration in solution.

Here, we report uniform and dispersive $CaCO_3$ nanoparticles synthesized using apoferritin by repeated CO_2 pressurization and depressurization, and show that control of the pH of the solution is important. We also calculate the electrostatic potential of apoferritin at various pH values to explain the mechanism of mineralization.

EXPERIMENTAL SECTION

Materials. Apofer-0 and apofer-8 were expressed in *Escherichia coli* cells as reported previously[13] and purified by ion-exchange chromatography (Q-Sepharose HP, GE Healthcare), gel-filtration chromatography (Sephacryl S-300 HR, GE Healthcare), and finally again by ion-exchange chromatography (MonoQ 10/100 GL, GE Healthcare). HSAF was purchased from Calbiochem and was purified by gel-filtration chromatography (Sephacryl S-300 HR, GE Healthcare). The protein concentrations of purified apofer-0, apofer-8, and HSAF were determined by absorbance at 280 nm using a value of 1.0 for 1 mg/mL protein.

Calcium carbonate ($CaCO_3$, ultra pure grade) was purchased from Sigma-Aldrich. It was crushed into 30 μm or smaller particles in a mortar to help its dissolution in water.

Isoelectric focusing (IEF) gels (Novex pH 3−7), anode buffer (Novex), cathode buffer (Novex pH 3−7), sample buffer (Novex pH 3−7), and protein marker (SERVA IEF Markers 3−10) were purchased from Invitrogen.

Isoelectric Point (pI) Measurements of Apofer-0, Apofer-8, and HSAF. The pI values of apofer-0, apofer-8, and HSAF were determined by isoelectric focusing (IEF). Each protein (2 μg) and marker proteins were applied on the IEF gel. Electrophoresis was performed at 100 V for 1 h, then 200 V for 1 h, and finally 500 V for 30 min, and then the gel was stained with Coomassie brilliant blue R-250. The pI values were calculated from a calibration curve made by plotting the distance moved by each marker protein versus the pH value.

Ca Mineralization in the Apoferritin Cavity Under CO_2 Gas Pressure. Ground $CaCO_3$ (less than 10 mg) was suspended in water, and then apoferritin solution (apofer-0, apofer-8, or HSAF) was added to give a protein concentration of 0.5 mg/mL and a total volume of 3 mL. A white, turbid suspension was obtained because the solubility of $CaCO_3$ is 0.13 mM under atmospheric pressure at room temperature. If 10 mg of $CaCO_3$ had dissolved completely in the solution, the concentration of $CaCO_3$ would have been 33 mM. The pH of the reaction solution was not controlled with buffer solution to allow changes in pH. The pH of the reaction solution was checked using either a pH meter or pH indicator solution. The sample solution was placed in a homemade airtight chamber (24 cm^3) and pressurized with gaseous CO_2 at 2 MPa for 1 h. The $CaCO_3$ suspension became transparent and colorless after 10 min. After 1 h at 2 MPa, the chamber was depressurized to ambient atmospheric pressure. This pressurization/depressurization cycle was repeated twice. Finally, the pressure was kept at 2 MPa for 1 day and then reduced to atmospheric pressure. After 1 h at ambient pressure, a small amount of white precipitate was formed. Most of the precipitate was removed by centrifugation at 7,000 g for 3 min, yielding a transparent, colorless supernatant. All processes were carried out at room temperature.

Transmission Electron Microscope (TEM) Observation and Energy Dispersive X-ray (EDX) Analysis. The synthesized nanoparticles were confirmed using a TEM (1200EX, JEOL) operated at 80 kV with and without negative staining. Aurothioglucose was used as a staining agent. Since aurothioglucose does not penetrate the apoferritin cavity and stains only the outside of the apoferritin molecule, apoferritin and ferritin (apoferritin containing nanoparticles) could be distinguished.[13] Aurothioglucose powder was directly added in the solution to not dilute the solution. Using negatively stained TEM images of the resultant solution, the efficiency of nanoparticle formation (ENF), defined as the ratio of the number of ferritin molecules to the total number of protein molecules, was evaluated.

EDX analysis was performed to examine the elemental composition of the synthesized nanoparticles. Unstained TEM samples were prepared and observed in the scanning transmission mode (STEM) of a high resolution TEM (JEM-2100F, JEOL) operated at 200 kV. The electron diffraction pattern of the synthesized nanoparticles was also observed with high resolution TEM to examine the crystal structure of the synthesized nanoparticles.

Evaluation of Particle Size. The particle size of individual synthesized nanoparticles was determined with imaging analysis software (Sumitomo Metal Technology Inc.) that calculates particle size from the area of the particle. The particle size distribution and average particle size of the synthesized nanoparticles were determined from the particle-size data.

Electrostatic Potential Calculations. The electrostatic potential distribution of apoferritin molecules at various pH values (pH 4.4, 6.5, and 9.3) were examined. Apoferritin is a fairly large molecule, with ionizable residues whose charges change according to the pH. Thus, using a straightforward molecular level simulation of this large protein−solvent system to obtain the electrostatic potential of apoferritin would require an enormous amount of calculation time, so we used a continuum electrostatic model instead.[14]

The atomic coordinates of the L-subunit of horse ferritin were obtained from the Protein Data Bank at Osaka University (accession code 1IER).[15] As the 1IER data set contains only the monomer subunit and lacks the hydrogen atom coordinates, the hydrogen coordinates were generated using Discovery Studio software (Accelrys Inc.). The full 24-mer molecule was constructed from the *F*432 symmetry written in the 1IER data set. In this calculation, the eight N-terminal residues of each subunit were deleted to emulate the apofer-8 structure. Each subunit of L-apoferritin, which lacks the eight N-terminal residues, contains ionizable groups: 28 acidic groups (12 Asp, 15 Glu, and the C-terminus) and 26 basic groups (10 Arg, 9 Lys, 6 His, and the N-terminus). In the calculation, the ionization of Lys and Arg residues was not considered because they were assumed to be charged at all pH values investigated in this calculation. The pK_a of every ionizable group at each specific pH was determined to minimize the electrostatic free energy of the system, based on the Tanford−Roxby approximation.[14] The intrinsic p*K* values of Nozaki and Tanford[16] were used. All atomic charges of the apoferritin 24-mer molecule were then determined.

The electrostatic potential was calculated as previously described.[17−19] Specifically, we calculated the electrostatic free energy at each pH by considering every ionizable residue. The solvent accessible boundary was determined by tracing a water molecule of radius 0.14 nm over the protein walls. This boundary was employed in the solution of the Poisson equation. The Poisson−Boltzmann (PB) equation was solved using the Debye parameter, $\kappa = 1\ nm^{-1}$, which is the appropriate value for a 30 mM $CaCl_2$ electrolyte solution. Because the potential quickly diminishes to zero outside the protein, use of the linear PB equation is justified.

In the initial calculations, all the ionizable acidic and basic residues in apoferritin were assumed to be neutral. The electrostatic free energy of the system at a given pH was calculated iteratively by changing the charge of all ionizable groups in the apoferritin 24-mer. Charge parameters were obtained from the CHARMM22 force field.[20] The dielectric constant of the protein was set to 4, which appears to be a more appropriate value for proteins than the typical hydrocarbon value of 2.[21]

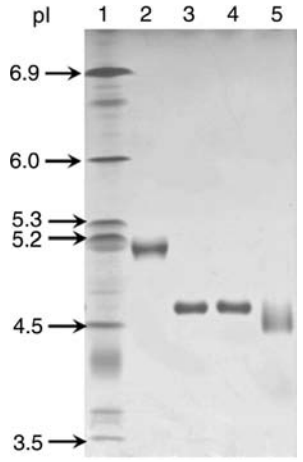

Figure 1. Coomassie blue stained pI profiles. Lanes 1 to 5 correspond to protein maker (SERVA), apofer-0, apofer-8, apofer-8 without NaCl, and HSAF, respectively. The pI value of apofer-0, apofer-8, and HSAF were determined by interpolating the pI values of the protein makers, and were determined to be 5.1, 4.7, and 4.4−4.6, respectively.

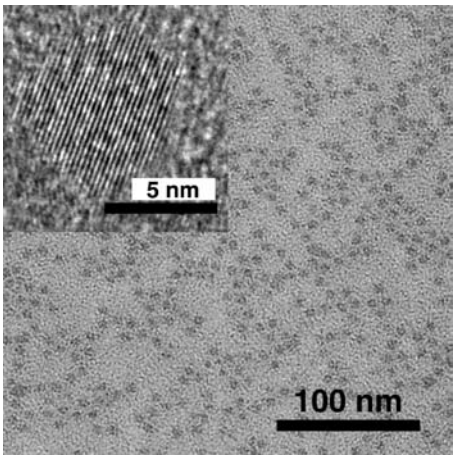

Figure 2. Unstained TEM image of the formed nanoparticles. The formed nanoparticles inspected by TEM were nearly spherical, uniform particles. A high resolution TEM image of a nanoparticle is shown in the inset. The lattice spacing determined from the high resolution image was 0.24 ± 0.02 nm.

A value of 77 was employed for the dielectric constant in the PB region ($\kappa = 1\ nm^{-1}$), as described earlier.[19] The Poisson and PB equations were solved using a finite difference method. A grid size of 0.1 nm and room temperature ($T = 298$ K) were used for all calculations.

The calculations were carried out on the HPC cluster at Ritsumeikan University, and the SGI Altix4700 and Fujitsu PRIMEQUEST supercomputers at Okazaki Research Facilities.

RESULTS

Isoelectric Point (pI) Analysis. IEF was performed to determine the pI of apofer-0, apofer-8, and horse spleen apoferritin (HSAF). Apofer-0 (Figure 1, lane 2) and apofer-8 (Figure 1, lanes 3 and 4) provided sharp single bands, but HSAF (Figure 1, lane 5) provided a diffuse band. This difference was expected given the heterogeneity of the HSAF subunits. HSAF is a hetero-oligomer of H- and L- subunits, whereas apofer-0 and apofer-8 consist only of L-subunits. The content of the H-subunit in HSAF is not fixed, but is distributed in the population and averages about 15%.[5] For this reason, the IEF band of HSAF would be rather broad. By interpolating between the pI values of the protein markers, the pI values of apofer-0, apofer-8 and HSAF were determined to be 5.1, 4.7, and 4.4−4.6, respectively. The L-subunit of apofer-8 lacked the eight amino acids at the N-terminus; since this deleted peptide contains one arginine residue, the apofer-8 molecule lacks 24 arginine residues compared to apofer-0. The elimination of these arginine residues lowers the pI value of apofer-8 compared to apofer-0. Since the L-subunit of natural ferritin (HSAF) also lacks this N-terminal fragment, the L-subunit of HSAF and apofer-8 might have identical pIs. The pI value of the horse H-subunit must be lower than that of the L-subunit because the pI value of HSAF, which contains H-subunits, is lower than that of apofer-8.

Optimization of Conditions for Ca Mineralization. To examine the Ca mineralization ability of the different subunits, the efficiency of nanoparticle formation (ENF) in apofer-0, apofer-8, and HSAF was examined. Apoferritin was added to the $CaCO_3$ solution (10 mg $CaCO_3$ in 3 mL of water). The ENF of apofer-0 and apofer-8 was about 50% and 70%, respectively, whereas no nanoparticle formation was observed in HSAF. We concluded that the ENF was highest when apofer-8 is used as the template.

To determine the optimal Ca concentration for the Ca mineralization process, solutions with various Ca concentrations (1, 5, 10 mg $CaCO_3$ in 3 mL of water) were tested. Because the maximum mass of $CaCO_3$ soluble in 3 mL of water at 2 MPa CO_2 gas pressure is about 10 mg, Ca concentration was varied below this concentration. Apofer-8 was used for Ca mineralization. The ENF was 40% at 5 mg of Ca in 3 mL of water, whereas no nanoparticle formation was observed at 1 mg Ca in 3 mL of water. The highest ENF was 70% at 10 mg Ca in 3 mL of water.

Apoferritin sometimes precipitates during the mineralization of metal ions,[13] perhaps because divalent cations can bridge apoferritin molecules. However, in our experiments, apoferritin did not precipitate even at high Ca concentrations. This may be due to the low affinity of Ca ions for the apoferritin cation binding site at the surface of the molecule.

To examine the change in pH during the mineralization process, the pH was checked with a pH meter and pH indicator dyes. Before pressurization, the pH of the reaction solution was 9.3. Under pressure, the pH of the solution was examined using the indicators methyl red (MR) and methyl orange (MO). The pH range of the color transition for MR and MO is 4.4−6.2 and 3.1−4.4, respectively. Under CO_2 pressurization, the reaction solution containing MR changed color, indicating a pH below 4.4, whereas the reaction solution containing MO did not change color, indicating a pH above 4.4. Given the color of the two pH indicators, the pH of the reaction solution during pressurization was determined to be about 4.4. After the solution stood at atmospheric condition for 1 h, the pH of the reaction solution increased to 6.5.

When argon (Ar) gas was used instead of CO_2 gas, the pH remained at or above 8.0, and the $CaCO_3$ did not dissolve. When a buffer solution, 200 mM HEPES (pH 7.0), was added to the reaction solution, the pH did not decrease below 5.3 even following CO_2 pressurization, and no nanoparticle formation was observed. Nanoparticle formation was only observed when nonbuffered solution was pressurized using CO_2 gas. These results indicate that CO_2 pressurization, causing a decrease in pH, is crucial for Ca nanoparticle formation in the apoferritin cavity.

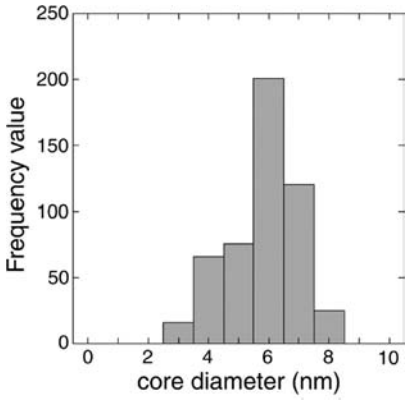

Figure 3. Size-distribution of the formed nanoparticles. The diameters of the nanoparticles were determined using 505 nanoparticles in the unstained TEM image. The average diameter was 5.8 ± 1.2 nm.

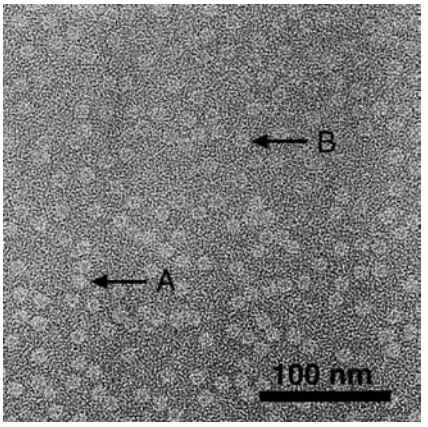

Figure 4. Negatively stained TEM image of ferritin and apoferritin. The white disks correspond to apoferritin protein (indicated by (A)), and the dense dots with white rings correspond to apoferritin containing nanoparticles (indicated by (B)). The efficiency of core formation was 70%.

The above results indicate that the best condition for Ca mineralization is apofer-8 (0.5 mg/mL) and $CaCO_3$ (10 mg in 3 mL of water) pressurized repeatedly with gaseous CO_2 at 2 MPa.

Characterization of the Formed Nanoparticles. Nanoparticles formed under the optimized condition were inspected by TEM with and without 2% aurothioglucose. Nearly spherical and uniform particles were observed in the unstained TEM image (Figure 2). To evaluate their size distribution, 505 nanoparticles from the unstained TEM image were analyzed (Figure 3) and provided an average diameter of 5.8 ± 1.2 nm.

White disks and dense dots surrounded by white rings were observed in the negatively stained TEM image (Figure 4). The white disks correspond to apoferritin protein (Figure 4A), while the dense dots correspond to nanoparticles surrounded by a protein shell (Figure 4B). These results indicate that the nanoparticles were formed in the apoferritin cavity. The ENF was about 70%. The nanoparticles formed in the apoferritin cavity were uniform and dispersive, since the nanoparticles are surrounded by protein shells that prevent aggregation.

EDX analysis was performed to examine the elemental composition of the nanoparticles formed in the apoferritin cavity. A STEM image of an unstained sample is shown in Figure 5A.

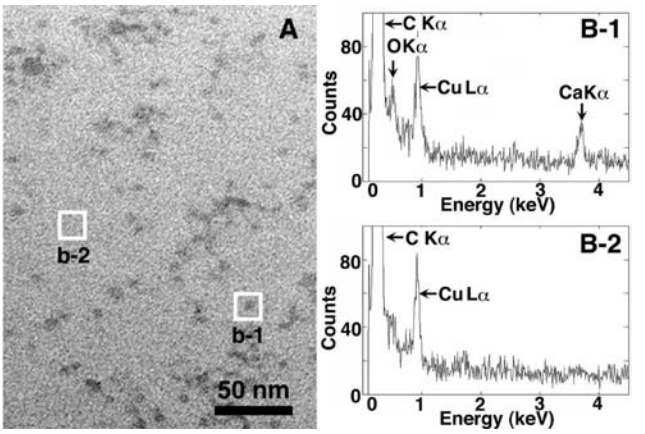

Figure 5. EDX analysis of the formed nanoparticles. Unstained STEM image of nanoparticles (A), and EDX spectra at area b-1 (B-1) and area b-2 (B-2). Peaks due to calcium (Kα; 3.7 keV) and oxygen (Kα; 0.53 keV) were detected only at areas containing a nanoparticle.

EDX analysis was performed on the area containing nanoparticles (area b-1 in Figure 5A) and a control area without nanoparticles (area b-2 in Figure 5A). Calcium (Kα; 3.7 keV), oxygen (Kα; 0.53 keV), carbon (Kα; 0.28 keV), and copper (Kα; 8.04 keV, Kβ; 8.90 keV, Lα; 0.93 keV) were detected in the area containing nanoparticles (Figure 5B-1), whereas only carbon and copper were detected from the control area (Figure 5B-2). The copper peaks arose from the TEM grid. These results indicate that the formed nanoparticles contain calcium and oxygen.

The crystal structure of the formed nanoparticles was examined using selected-area electron diffraction. The observed *d*-spacings of the synthesized nanoparticles were 0.304, 0.220, and 0.186 nm, which are consistent with the (1 0 4), (2 0 2), and (1 1 6) Miller indices of calcite, a $CaCO_3$ polymorph.

Electrostatic Potential Calculations. The electrostatic potential around the apoferritin molecule was calculated at pH 4.4, 6.5, and 9.3. The electrostatic potential and the electric field in the cross-section involving 4-fold, 3-fold, and 2-fold symmetry axes are shown in Figure 6. This cross-section contains 4 3-fold channels and 2 4-fold channels (Figure 6A). The electrostatic potential profile along the 3-fold symmetry axis and 4-fold symmetry axis at each pH is shown in Figure 7. The potential inside the cavity is negative at pH 6.5 and pH 9.3 (Figures 6C and D, Figure 7), but turns positive at pH 4.4 (Figure 6B, Figure 7).

The 3-fold channels are negatively charged between pH 4.4 and pH 9.3 because the channels are rich in acidic amino acids. Thus, the electric field in the 3-fold channel is always directed toward the center of the channel (Figure 6, Figure 7A). The electric field at the outer entrance of the 3-fold channel is also directed toward the inside at pH 6.5 and pH 9.3, but is reduced to almost zero at pH 4.4 (Figure 7A). The negative potential wall at the 3-fold channel decreases with decreasing pH (Figure 7A), and at pH 4.4 it is about half its value at pH 6.5.

The 4-fold channels are mainly lined with hydrophobic amino-acid residues, although histidine residues are located at the entrance of the cavity side (Figure 6A). This contributes positive potential in the 4-fold channel at pH 4.4 and pH 6.5 (Figure 7B), and the electric field is directed toward the entrance of the channel. At pH 9.3, the histidine residues are not protonated and the direction of the electric field becomes complicated (Figure 7B).

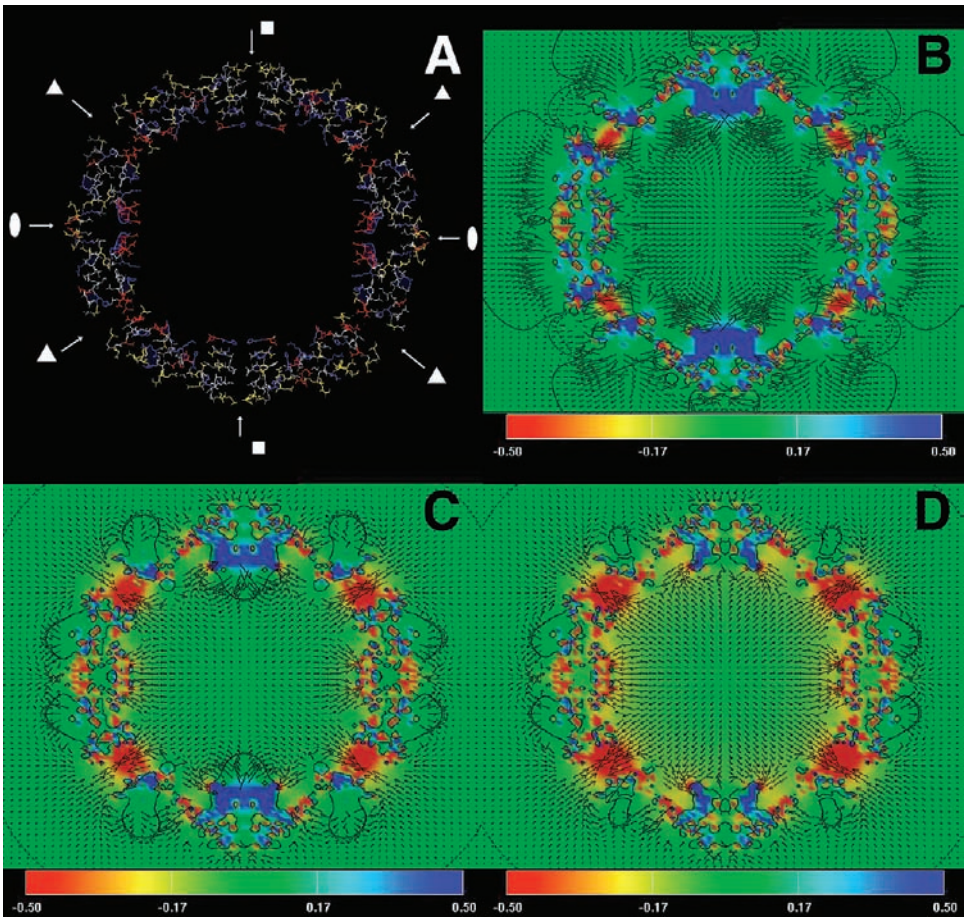

Figure 6. Calculated electrostatic potential distribution of apoferritin. A cross-section of an apoferritin molecule wire model (A), including the 2-fold symmetry axis (○), 3-fold symmetry axis (△), and 4-fold symmetry axis (□). Red indicates acidic amino acids, blue indicates basic amino acids, yellow indicates neutral amino acids, and gray indicates hydrophobic amino acids. The calculated electrostatic potential distribution of apoferritin at pH 4.4 (B), pH 6.5 (C), and pH 9.3 (D) are shown. The potential value (in volts) is expressed by colors as shown in the lower column of each figure. The direction and the strength of the electric field at the corresponding position are expressed by the vector in relative length.

DISCUSSION

Ca-NPs were synthesized in the cavity of apoferritin by repeated pressurization with gaseous CO_2. Under pressure, CO_2 tends to dissociate into H^+ and HCO_3^-; the resulting decrease in pH leads to increased $CaCO_3$ solubility. Then, the dissociated Ca^{2+} and HCO_3^- diffuse into the apoferritin cavity and mineralize.

The solubility of $CaCO_3$ is also increased by decreasing the temperature. We have reported $CaCO_3$ mineralization in the apoferritin cavity by heating and cooling saturated $Ca(HCO_3)_2$ solution.[22] It is believed that $CaCO_3$ crystal nuclei develop in the cavity when the solubility of $CaCO_3$ is altered.

The pH of the reaction solution is also important for nanoparticle generation in the apoferritin cavity. We have succeeded in generating nanoparticles by decreasing the pH (to pH 4.4) of the solution using CO_2 pressurization, whereas no nanoparticle formation was observed in buffered solution that prevented the pH from decreasing below 5.3. This can be explained by the change in the electrostatic potential of the inner (cavity) surface and outer surface of the apoferritin molecule. At pH 9.3, before pressurization, all acidic and basic amino acid side-chains except histidine are likely dissociated. According to the calculated electrostatic potential shown in Figure 6D, most of the external protein surface carries a negative potential, and the potential of the cavity surface is lower than the potential of the exterior surface (Figure 7). At neutral pH, the absolute value of the negative surface potential is decreased, but remains overall negative. Douglas and Ripoll[8] calculated the electrostatic potential of human H-apoferritin at neutral pH, and concluded that the electric field is directed from the outside to the inside of the 3-fold channel, thereby forcing the cation into the apoferritin cavity. A similar situation is observed in horse L-apoferritin (Figure 6C).

Cations in the 3-fold channel will be trapped in the center of the channel because the potential is lowest there. However, this potential will be reduced by the interaction of a divalent cation with the acidic amino acids in the channel, resulting in this cation being pushed into the cavity by the binding of the next cation.[18] In contrast to neutral or alkaline pH, at low pH (pH 4.4), the positive area is increased, especially on the inner surface (Figure 6B), primarily because of protonation of the numerous histidine residues on the inner surface (Table 1). Because the pI of the histidine side-chain is approximately 6, it is completely protonated at pH 4.4. The pIs of the acidic amino acids are about 4; therefore, they are about 70% to 80% dissociated at pH 4.4 and retain their negative charge. Since the total number of acidic amino acids on the surface of the cavity is larger than the number

dx.doi.org/10.1021/ic200117x |*Inorg. Chem.* 2011, 50, 6526–6532

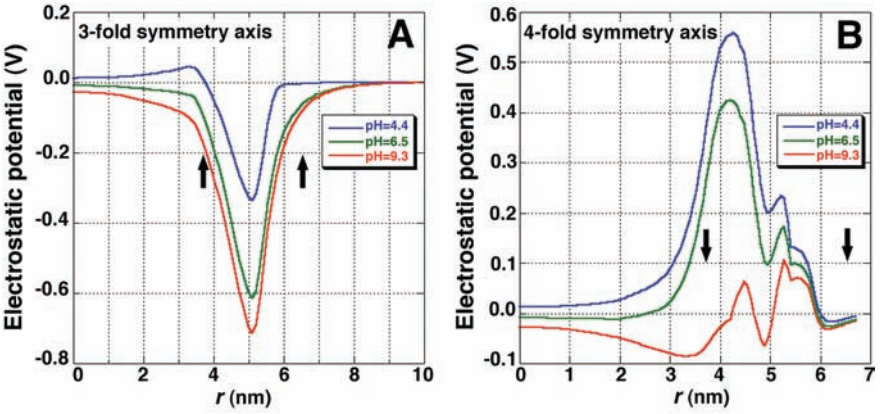

Figure 7. Electrostatic potential along the 3-fold and 4-fold symmetry axis. The pH dependence of the calculated electrostatic potential along the 3-fold symmetry axis (A) and 4-fold symmetry axis (B) at pH 4.4 (in blue), 6.5 (in green) and 9.3 (in red) is shown. The abscissa shows the distance from the center of the molecule. The arrows in the figure indicate the edge of the protein shell, with the inner surface at 3.7 nm and the exterior surface at 6.5 nm. The lines between these arrows indicate the electrostatic potential through the center of the channels.

Table 1. Number of Acidic and Basic Amino Acids in a L-apoferritin Subunit

	exterior surface	cavity surface
acidic amino acids	Asp ×7 Glu ×4	Asp ×5 Glu ×11
basic amino acids	Lys ×3 Arg ×6 His ×1	Lys ×6 Arg ×4 His ×5

on the outer surface, the reduction in negative charge is larger on the cavity surface; consequently, the electrostatic potential of the cavity is positive and higher than that of the outer surface at pH 4.4. The total charge on apofer-8 is positive at pH 4.4, since the pI value obtained by IEF was 4.7. Anions would be attracted into the cavity because of the cavity's positive potential at pH 4.4. The 4-fold channel, which has positive potential, may act as an anion pathway, although the surface of the channel is rich in hydrophobic amino acids. The conformational fluctuation of the subunits would help decrease this hydrophobic barrier. The 3-fold channel carries an overall negative charge; the potential barrier is lower at pH 4.4, and this may allow the entrance of anions.

In addition to these electrostatic aspects, the concentration of bicarbonate ions (HCO_3^-) increases when the CO_2 pressure is increased. Because of the difference in bicarbonate ion concentration inside and outside the cavity, pressurization will cause anions to accumulate further in the cavity. This can be explained by the difference in the total chemical potential, represented by the sum of the electro-chemical potential and the concentration. The bicarbonate ions trapped in the cavity will precipitate as $CaCO_3$ because of changes in the chemical potential after release of the CO_2 pressure.

No nanoparticle formation was observed when HSAF was used as a template, probably because of the H-subunit in HSAF. IEF showed that the pI value of HSAF is around 4.5, so the total charge on HSAF will be almost zero at pH 4.4, and thus the electrical potential difference would be insufficient to accumulate anions in the cavity.

The efficiency of nanoparticle formation in apofer-0 is lower than in apofer-8, although both consist only of L-subunits. The difference in these two molecules is the N-terminal residues located on the exterior surface. These are distant from the 3-fold channel and will not participate in mineralization. The N-terminus is believed to link neighboring subunits and help stabilize the apoferritin molecule in acidic conditions.[9] Therefore, structural fluctuations of the subunit will be larger in apofer-8 at acidic pH, thereby reducing the potential barrier in the ion channel formed at the intersubunit interface. Molecules larger than the diameter of the ion channel can sometimes mineralize in the apoferritin cavity. To explain this mineralization, Massover[23] proposed dynamic fluctuation of the ion channel. This fluctuation would decrease the potential barrier of the 3-fold or 4-fold channels and aid in the accumulation of ions.

After depressurization, the pH increased to 6.5, and the potential became almost neutral. Under these conditions, both cations and anions may be able to access the cavity, although acidic amino acids in the 3-fold channel would produce a negative potential barrier. Negative ions would therefore be unable to access the cavity, whereas the electric field would aid Ca^{2+} to enter the cavity through the 3-fold channels.

The electrostatic potential changes described above suggest that cations and anions would accumulate in the cavity and form insoluble compounds like calcium carbonate nanoparticles. However, this viewpoint is rather static, and we have to consider dynamic processes to really understand the mineralization process. For example, even one anion or cation accumulated in the cavity would change the potential map dramatically. A chemical reaction such as oxidation or reduction in the cavity would also induce a large change in potential. In the future, we will consider these dynamic processes to better understand apoferritin mineralization, but our current static viewpoint is nonetheless a good starting point for examining the mineralization process.

We have succeeded in generating $CaCO_3$ nanoparticles in the apoferritin cavity that have uniform size distribution. Control of the electrostatic potential of apoferritin is clearly important for this and other mineralization processes.

AUTHOR INFORMATION

Corresponding Author

*Phone: 81-44-934-7439. Fax: 81-44-900-0421. E-mail: yoshi@isc.meiji.ac.jp.

ACKNOWLEDGMENT

This study was partially supported by the Private Universities Foundation for the Development of Fundamental Research

Strategies, and the "Academic Frontier Project" from MEXT (the Ministry of Education, Culture, Sports, Science and Technology) of Japan. The calculation study was partly supported by the MEXT project "Water as a key player in ATP energy transduction", and the calculation was partly done on the supercomputers in the Research Center for Computational Science, Okazaki Research Facilities, and National Institute of Natural Sciences.

REFERENCES

(1) Heuer, A. H.; Fink, D. J.; Laraia, V. J.; Arias, J. L.; Calvert, P. D.; Kendall, K.; Messing, G. L.; Blackwell, J.; Rieke, P. C.; Thompson, D. H.; Wheeler, A. P.; Veis, A.; Caplan, A. I. *Science* **1992**, *255*, 1098–1105.
(2) Stupp, S. I.; Braun, P. V. *Science* **1997**, *277*, 1242–1248.
(3) Uchida, M.; Klem, M. T.; Allen, M.; Suci, P.; Flenniken, M.; Gillitzer, E.; Varpness, Z.; Liepold, L. O.; Young, M.; Douglas, T. *Adv. Mater.* **2007**, *19*, 1025–1042.
(4) Yoshimura, H. *Colloids Surf., A.* **2006**, *282*−*283*, 464–470.
(5) Harrison, P. M.; Arosio, P. *Biochim. Biophys. Acta* **1996**, *1275*, 161–203.
(6) Takeda, S.; Ohta, M.; Ebina, S.; Nagayama, K. *Biochim. Biophys. Acta* **1993**, *1174*, 218–220.
(7) Ford, G. C.; Harrison, P. M.; Rice, D. W.; Smith, J. M. A.; Treffry, A.; White, J. L.; Yariv, J. *Phil. Trans. R. Soc. Lond. B* **1984**, *304*, 551–565.
(8) Douglas, T.; Ripoll, D. R. *Protein Sci.* **1998**, *7*, 1083–1091.
(9) Yoshizawa, K.; Mishima, Y.; Park, S. Y.; Heddle, J. G.; Tame, J. R. H.; Iwahori, K.; Kobayashi, M.; Yamashita, I. *J. Biochem.* **2007**, *142*, 707–713.
(10) Douglas, T.; Stark, V. T. *Inorg. Chem.* **2000**, *39*, 1828–1830.
(11) Iwahori, K.; Yoshizawa, K.; Muraoka, M.; Yamashita, I. *Inorg. Chem.* **2005**, *44*, 6393–6400.
(12) Li, M.; Viravaidya, C.; Mann, S. *Small* **2007**, *3*, 1477–1481.
(13) Okuda, M.; Iwahori, K.; Yamashita, I.; Yoshimura, H. *Biotechnol. Bioeng.* **2003**, *84*, 187–194.
(14) Yang, A. S.; Gunner, M. R.; Sampogna, R.; Sharp, K.; Honig, B. *Proteins: Struct., Funct., Genet.* **1993**, *15*, 252–265.
(15) Granier, T.; Gallois, B.; Dautant, A.; Langlois d'Estaintot, B.; Precigoux, G. *Acta Crystallogr., Sect. D: Biol. Crystallogr.* **1997**, *53*, 580–587.
(16) Nozaki, Y.; Tanford, C. *Methods Enzymol.* **1967**, *11*, 715–734.
(17) Ootaki, M.; Endo, S.; Sugawara, Y.; Takahashi, T. *J. Cryst. Growth* **2009**, *311*, 4226–4234.
(18) Takahashi, T.; Kuyucak, S. *Biophys. J.* **2003**, *84*, 2256–2263.
(19) Takahashi, T.; Nakamura, H.; Wada, A. *Biopolymers* **1992**, *32*, 897–909.
(20) MacKerell, A. D., Jr.; Bashford, D.; Bellott, M.; Dunbrack, R. L., Jr.; Evanseck, J. D.; Field, M. J.; Fischer, S.; Gao, J.; Guo, H.; Ha, S.; Joseph-McCarthy, D.; Kuchnir, L.; Kuczera, K.; Lau, F. T. K.; Mattos, C.; Michnick, S.; Ngo, T.; Nguyen, D. T.; Prodhom, B.; Reiher, W. E., III.; Roux, B.; Schlenkrich, M.; Smith, J. C.; Stote, R.; Straub, J.; Watanabe, M.; Wiorkiewicz-Kuczera, J.; Yin, D.; Karplus, M. *J. Phys. Chem. B* **1998**, *102*, 3586–3616.
(21) Gilson, M, K.; Honig, B, H. *Biopolymers* **1986**, *25*, 2097–2119.
(22) Fukano, H.; Aizawa, M.; Yoshimura, H. *Key Eng. Mater.* **2008**, *361*−*363*, 183–186.
(23) Massover, W. H. *Micron* **1993**, *24*, 389–437.